JETIR.ORG ISSN: 2349-5162 | ESTD Year : 2014 | Monthly Issue
JOURNAL OF EMERGING TECHNOLOGIES AND INNOVATIVE RESEARCH (JETIR)
An International Scholarly Open Access, Peer-reviewed, Refereed Journal

RESIDENTIAL OCCUPANCY DETECTION USING PIR SENSOR NETWORKS

An attempt to create low cost residential true occupancy detection system

[1]Abdul Azeez Yasir, [2]Mohammed N.A Saqlain , [3]Nishaanth G, [4]Lalitha H

[1]Student, [2]Student, [3]Student, [4]Assistant Professor
[1]Department of Electronics and Instrumentaion Engineering
[1]Bangalore Institute of Technology, Bengaluru, Karnataka, India

Abstract : Passive infrared (PIR) sensors are the most popular deployed sensors in buildings for individual presence detection. However, PIR sensors are motion detectors in nature, responding only to incident radiation variation, which leads to false negative detections, inaccurate occupancy estimation, and uncomfortable lighting swings and waste of energy. To address this issue we demonstrate the use of previously developed chopped PIR (C-PIR) in a wired network of such sensor nodes.

IndexTerms **- Passive infrared sensor; Stationary occupancy detection; Motion detection; True occupancy detection; Wired sensor networks.**

I. INTRODUCTION

A. Background and Motivations

Detecting occupancy is crucial for managing power usage in both commercial and residential buildings. Utilizing occupancy information for lighting, heating, ventilation, and air-conditioning (HVAC) systems can significantly reduce energy consumption while maintaining user comfort. Two primary types of occupancy detection systems exist: terminal-based and non-terminal-based systems.

Terminal-based systems require a terminal such as a mobile phone or radio frequency identification (RFID) tag. These terminals must be carried by occupants, leading to high deployment costs, privacy concerns, and inconveniences. On the other hand, non-terminal-based occupancy detection systems encompass various technologies, including passive infrared (PIR) sensors, carbon dioxide (CO2) sensors, ultrasonic sensors, image recording devices, and thermopile array sensors.

CO2 sensors gauge gas concentration in the environment to predict occupancy information related to presence and counting. However, they are susceptible to environmental factors like wind speed, sensor placement, and airflow. Ultrasonic sensors measure echo intensity to determine presence and location but often encounter false positives due to environmental vibrations. Image-based detection systems, like video cameras, are widely used for occupancy detection, offering presence, localization, identification, and activity tracking capabilities. Nonetheless, they require adequate lighting, precise sensor positioning, costly hardware, complex signal processing, and raise privacy concerns.

Thermopile array sensors, featuring multiple thermopile detectors responsive to received radiation through the Seebeck effect, offer presence, localization, and facing direction detection. However, they are more expensive, have shorter detection ranges, and smaller fields of view (FOV) compared to PIR sensors.

B. PIR Sensors: Advantages, and Major Drawbacks

PIR sensors stand as the predominant choice for detecting occupancy presence in the majority of buildings. These sensors are extensively employed for regulating lighting, heating, and cooling based on occupancy information, primarily due to their affordability, low energy consumption, extensive detection range, broad field of view (FOV), and dependable performance. By detecting fluctuations in heat flux, PIR sensors effectively respond to variations in radiation energy. Occupancy detection systems based on PIR sensors offer insights into presence, localization of multiple occupants, tracking, movement direction, and identification.

Nevertheless, a significant challenge lies in the inherent nature of PIR sensors as motion detectors, limiting their ability to detect stationary occupants. This inherent limitation results in frequent false negatives, leading to discomfort caused by lighting or temperature fluctuations and wastage of power.

II. CHOPPED PIR SENSOR

Various commercial and emerging technologies are available for occupancy sensing, including optical cameras and methods utilizing ultrasonic, radio frequency, or thermal infrared sensing. However, many of these options tend to be costly, require multiple sensor nodes, or raise privacy concerns. Pyroelectric infrared (PIR) sensors have emerged as the preferred choice for occupancy estimation due to their cost-effectiveness, low energy consumption, extensive detection range, wide field of view (FOV), and reliability. These sensors are commonly utilized for tasks such as occupancy presence inference, multiple occupancy localization and tracking, movement direction detection, and person identification.

However, PIR sensors are inherently limited to motion detection since they only respond to fluctuations in radiated heat, stemming from their nature as motion detectors. Additionally, most commercial PIR sensors are equipped with sensing elements in pairs connected serially with opposite polarity, rendering them insensitive to stationary occupants. Despite attempts to address this issue by introducing opaque optical choppers to shutter radiated power, existing methods often suffer from limitations in detecting stationary occupants or result in high false-positive detection errors.

To overcome these challenges, this letter introduces a novel chopped PIR (C-PIR) sensor, as depicted in Figure 1(a), capable of accurately detecting both stationary and moving occupants. The C-PIR sensor incorporates a narrow infrared semi-transparent chopper to periodically shutter incident radiation. Its components include a commercial PIR sensor with dual sensing elements, an oscillating chopper with a driver, a Fresnel lens, an amplifier, and a microcontroller unit (MCU). The oscillating chopper selectively shutsters radiant power received by the dual sensing elements, allowing omnidirectional power from ambient sources to bypass the chopper when unoccupied. However, when occupied, the chopper effectively chops radiated heat emitted by occupants in one direction, resulting in a significantly higher output voltage indicative of occupant presence, regardless of whether they are in motion. Figure 1(b) illustrates the relationship between output voltage response R_U and input power W_0, expressed as the output voltage U_0 per watt of input power W_0.

$$R_u = \frac{U_0}{W_0} = \frac{s_{const}\omega}{\sqrt{(1+\omega^2\tau_T^2)(1+\omega^2\tau_E^2)}} \tag{1}$$

Where ω represents the angular frequency of the radiated power; τ_T and τ_E denote the thermal and electrical time constants, respectively; and Sconst = $AR_G\eta p_\perp/G_T$ is the constant characteristic of each specific PIR sensor [as depicted in Fig. 1(b)]. Here, G_T stands for the thermal conductance to the ambient, η represents the emissivity of the pyroelectric element, $p_\perp$ signifies the normal direction pyroelectric coefficient, R_G denotes the resistance of the gate, and $A = l_e w_e$ represents the sensing area. In Figure 1(c) (top view) and Figure 1(d) (front view) of the C-PIR sensor, the trajectory of the chopper within one chopping period ($t_{LD} - t_{RA}$) is illustrated. The time instants t_{RA}, t_{RB}, t_{RC}, t_{RD}, t_{LA}, t_{LB}, t_{LC}, and t_{LD} indicate when C_R and C_L reach positions A, B, C, and D, respectively.

$$W(t) = \begin{cases} \Phi_h w_e[2l_e - v_c t(1-\kappa_{ch})]; & t_{RA} \le t < t_{RB} \\ \Phi_h w_e l_e(1+\kappa_{ch}); & t_{RB} \le t < t_{RC} \\ \Phi_h w_e[2l_e + (l_s - v_c t)(1-\kappa_{ch})]; & t_{RC} \le t < t_{RD} \\ 2\Phi_h w_e l_e \kappa_{ch}; & t_{RD} \le t < t_{LA} \\ \Phi_h w_e[(1-\kappa_{ch})(v_c t - l_c) + 2l_e\kappa_{ch}]; & t_{LA} \le t < t_{LB} \\ \Phi_h w_e l_e[1+\kappa_{ch}]; & t_{LB} \le t < t_{LC} \\ \Phi_h w_e[(1-\kappa_{ch})(v_c t - l_c - l_s) + 2l_e\kappa_{ch}]; & t_{LC} \le t < t_{LD}. \end{cases} \tag{2}$$

In the above equation, l_c represents the width of the chopper; l_e and we represent the length and width of the sensing element, respectively; l_s represents the space between the two sensing elements; v_c represents the chopping speed. The ideal waveforms of W(t) of each chopping period are shown as solid lines in Fig. 1(e).

Only the variation of the incident power can induce the output voltage change. The variation of the incident power can be denoted as $\Delta W(t)$ and can be equivalent as a sinusoidal function with a period T=($t_{LD} - t_{RA}$)and an amplitude of $\phi_h\omega_e l_e(1-k_{cH})$.

$$\Delta W(t) = \phi_h\omega_e l_e(1-k_{cH})\sin[\frac{2\pi t}{T}] \tag{3}$$

When unoccupied, $\Delta W(t)$ radiated from the ambient is usually very small, as illustrated by the dashed line in Fig. 1(e). Figure 1(f) shows the voltage output corresponding to $\Delta W(t)$. The peak-to-peak (P-P) voltage value U_{ppe} induced by the ambient

radiation should be measured beforehand as the prerequisite information. When in operation, the P-P value U_{ppm} from the C-PIR sensor will be compared with U_{ppe} as the detection criteria: if ($U_{ppm} - U_{ppe}$) > U_{th}, where U_{th} is the threshold value, a moving or a stationary occupant will be detected; otherwise, an unoccupied scenario is indicated.

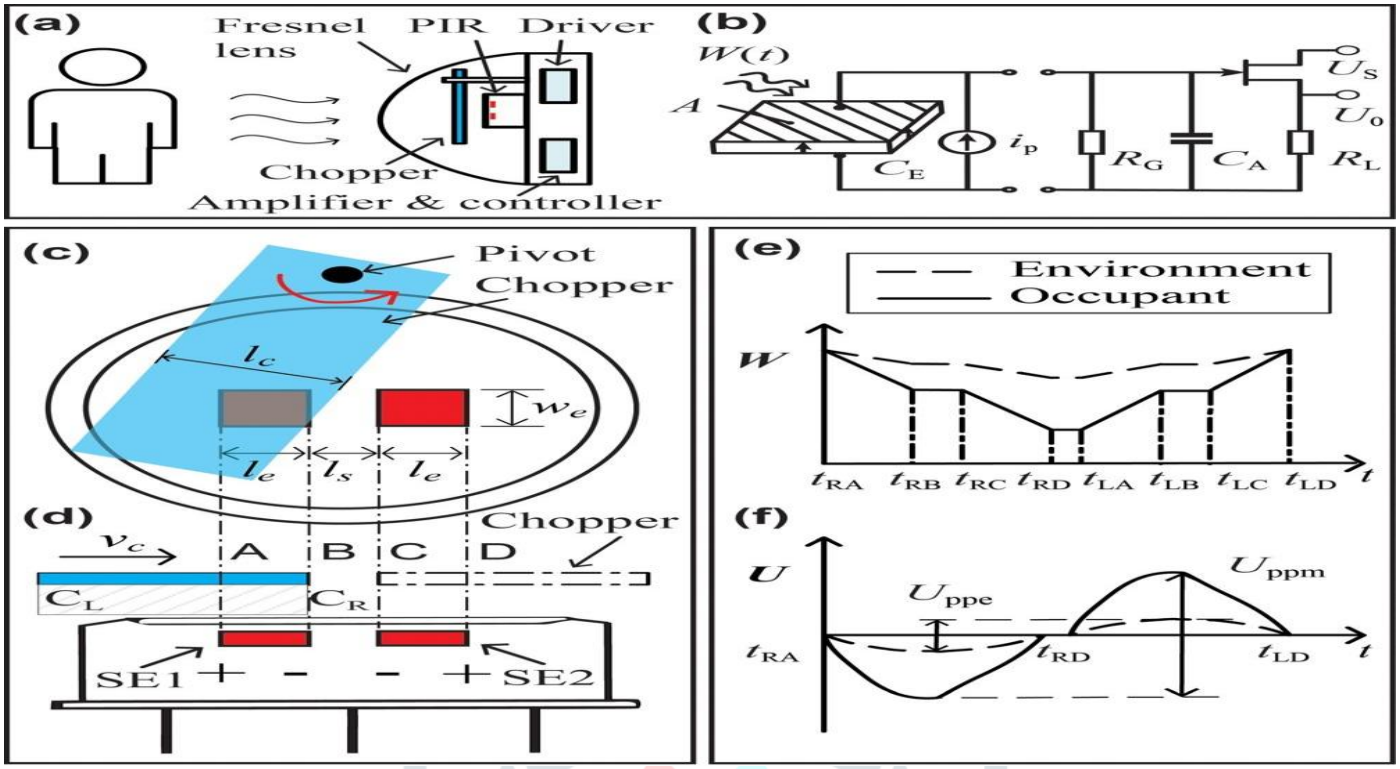

FIG. 1. (a) Schematic diagram of the C-PIR sensor; (b) one sensing element is radiated by the varying power (left) and a voltage source follower (right); R_L is the resistance of the gate and the load; C_E and C_A represent the capacitance of the sensing element and the amplifier; i_p is the current output of the pyroelectric element; U_S is the voltage supply; (c) the top view and (d) the front view of the C-PIR sensor; (e) the variation of the radiated power on the dual sensing elements; (f) the output voltage from the dual pyroelectric elements (not an ideal sinusoid waveform).

Equation (3) implies that both the transmittance and chopping speed can impact the radiated power, consequently influencing sensing performance. Hence, a parametric study is conducted to determine their optimal values. High-density polyethylene (HDPE) plastic is chosen as the chopper material for its optimal transmission bandwidth ranging from 7 µm to 13 µm. A chopper width of 2.0 mm is selected, slightly wider than that of the sensing element array.

The initial test involves an occupant with a skin temperature of 36°C positioned in front of the C-PIR sensor, utilizing a 1 mm thick chopper. The output voltage waveform depicted in Figure 2(a) illustrates two peak variations in opposite flow directions across two chopping periods, confirming the chopping principle depicted in Figures 1(c) and 1(d). Notably, Figure 2(a) reveals that the peak-to-peak value of the C-PIR sensor under an unoccupied scenario (U_{ppe} = 0.4 V) exceeds that of its PIR counterpart (0.12 V). When a stationary occupant is present at a distance of 1 m, the peak-to-peak value significantly increases for the C-PIR sensor (U_{ppm} = 4.6 V), while its almost unchanged for the PIR sensor (0.12 V).

Furthermore, Figure 2(b) illustrates the significant variation of U_{ppm} with changing chopping periods, indicating the potential for obtaining an optimal chopping frequency for a specific chopper in use, which will be examined in subsequent experiments.

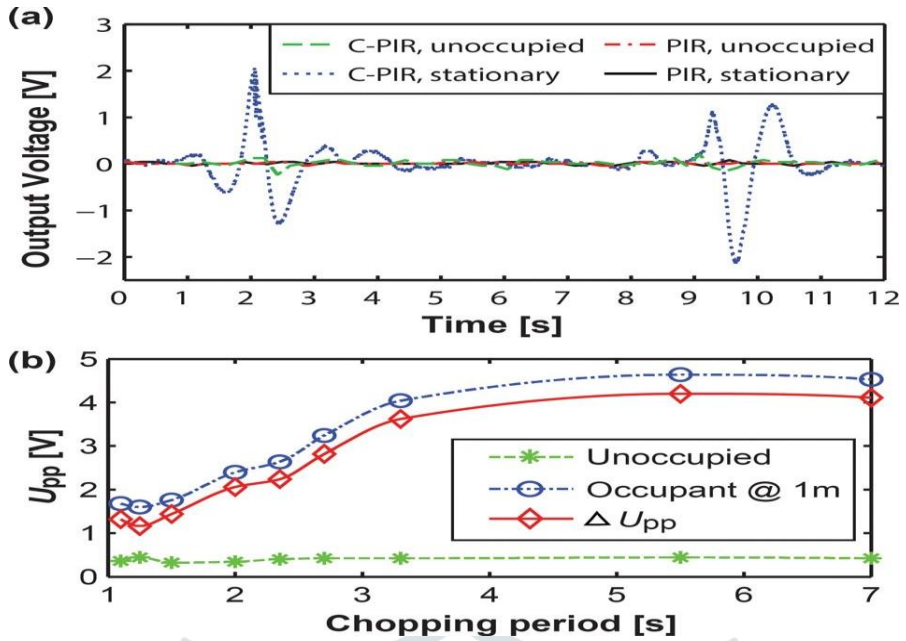

FIG. 2. (a) Output voltage waveforms induced by the C-PIR and its PIR counterpart when unoccupied and occupied by an occupant sitting at 1-m away, at the chopping period of 7 s; (b) P-P voltage outputs of the C-PIR when unoccupied and occupied by an occupant sitting 1-m-away at different chopping periods, where a 1 mm thick chopper is used.

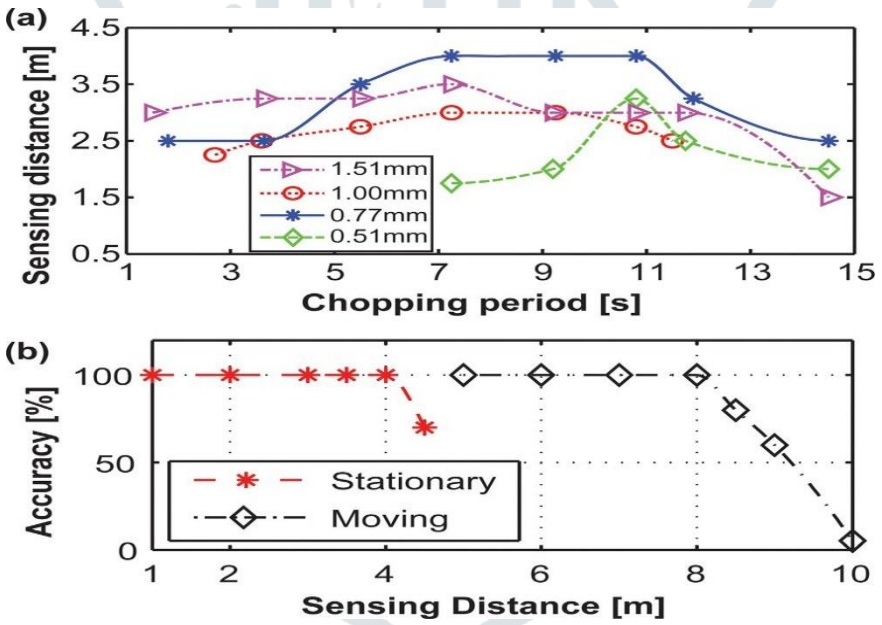

FIG. 3. (a) Longest sensing distance of a stationary occupant at different chopping periods; (b) accuracy testing on a stationary occupant and a moving occupant at different detection positions. Each marker represents 20 data tested at different times of the day in two different testing rooms.

Figure 3(a) displays the test results utilizing choppers of varying thicknesses (1.51 mm, 1 mm, 0.77 mm, and 0.51 mm) at an ambient temperature of 21.7°C and different chopping speeds. Notably, U_{ppe} fluctuates with the chopper thickness and chopping speed. A pre-defined ambient-dependent threshold value, U_{th} = max(1.6*U_{ppe}, U_{ppe}+0.2 V), is established. The results indicate the maximum detection range at different chopping periods associated with their respective predefined Uth values. Three choppers exhibit flat peaks, suggesting a broader range of optimal chopping speeds. The C-PIR sensor with a 0.77 mm thick chopper achieves a detection range of 4 m at optimal chopping periods ranging from 7 to 11 s, indicating the widest bandwidth of optimal chopping frequencies and thus selected for further performance characterization.

In Figure 3(b), accuracy evaluations of a C-PIR sensor with a 0.7 mm thick chopper at a chopping period of 7.5 s are presented for both stationary and moving occupancy detections. The testing spanned two days with ambient temperatures ranging from 24.9°C to 25.5°C and U_{th} = 1.6*U_{ppe} = 0.64 V. For stationary occupancy detection, an occupant positioned at distances of 1 m, 2 m, 3 m, 3.5 m, 4 m, and 4.5 m from the C-PIR sensor underwent 20 datasets collected for each range. A 100% accuracy rate is achieved for a range of up to 4 m (totaling 100 datasets), with accuracy dropping to 65% for a range of 4.5 m. For moving occupancy detection, the same occupant moved randomly at a speed of approximately 0.5 m/s at distances of 5 m, 6 m, 7 m, 8 m, 8.5 m, 9 m, and 10 m away. The C-PIR sensor maintains 100% accuracy within an 8 m range (totaling 80 datasets), with accuracy dropping to 75% (and below) for distances beyond 8.5 m.

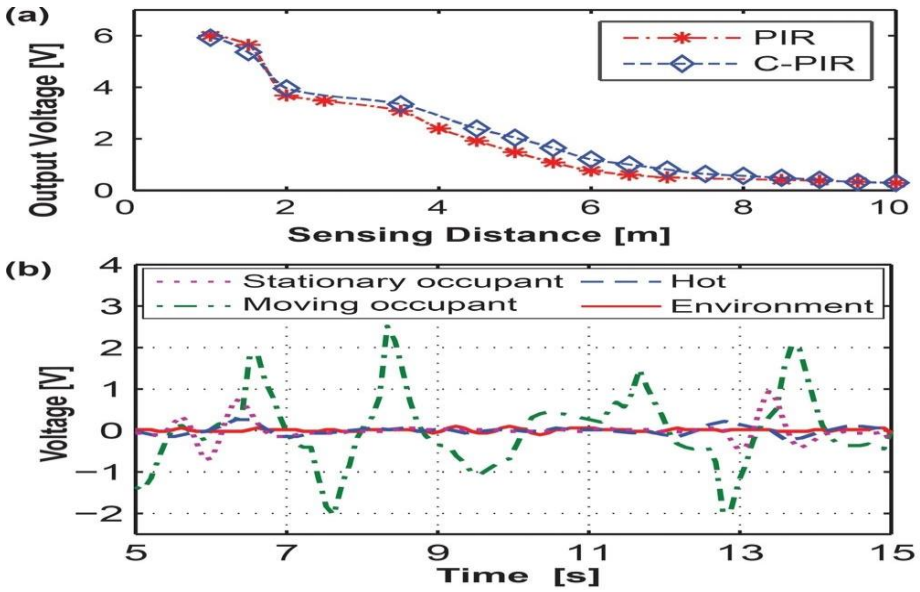

FIG. 4. (a) Output voltage results from a moving occupant in front of the traditional PIR and the C-PIR sensor; (b) voltage waveforms from the C-PIR sensor in terms of four scenarios: a stationary occupant at 2.5 m away; a moving occupant at 2.5 m away; a hot object at 2.25 m away; and ambient environment (no other hot object except for fluorescent lamps)

Figure 4(a) illustrates the peak-to-peak voltages from the C-PIR sensor across different detection ranges compared to their PIR counterparts, indicating similar output voltages for both sensors during moving occupancy detection.

In Figure 4(b), voltage waveforms of the C-PIR sensor are depicted under four scenarios: a stationary occupant positioned 2.5 m away, a moving occupant also at 2.5 m, a hot object with a temperature of 96.2°C placed at 2.25 m, and the distinction between these scenarios. Notably, a hot object positioned at 2.25 m does not induce a voltage higher than the threshold value (U_{th} = 0.64 V) at distances of 2.5 m or greater, hence the placement for comparison.

The field of view (FOV) of the C-PIR sensor is evaluated for both stationary and moving occupancy detection, compared with the traditional PIR counterpart. Supplementary materials provide the results, indicating that the FOV of the C-PIR sensor matches that of the on-board PIR sensor module, measuring 110 degrees horizontally and 90 degrees vertically. The C-PIR sensor demonstrates the capability to detect stationary occupants within a range of up to 4 m and moving occupants up to 8 m (matching the traditional PIR counterpart) with an accuracy of 100%.

III. SUMMARY

In summary, a prototype of the chopped Pyroelectric Infrared (C-PIR) sensor has been developed to detect both stationary and moving occupants. This sensor utilizes a narrow infrared semi-transparent chopper to modulate the incident radiation received by the pyroelectric sensing elements. Various prototypes of the C-PIR sensor with different chopper parameters have been compared through experimental testing. The findings demonstrate that the C-PIR sensor achieves high accuracy in detecting both stationary and moving occupants, with minimal influence from the narrow infrared semi-transparent chopper on the output voltage induced by moving occupants. Specifically, the sensor achieves 100% accuracy in detecting stationary occupancy up to 4.0 m and moving occupancy up to 8.0 m. The field of view (FOV) of the C-PIR sensor is determined to be 110 degrees horizontally and 90 degrees vertically, consistent with that of the on-board PIR sensor.

IV. REFERNCES

[1] T. A. Nguyen and M.Aiello, “Energy intelligent buildings based on user activity: A survey,” Energy Buildings, vol. 56, pp. 244–257, Jan. 2013.

[2] M. Asif ul Haq et al., “A review on lighting control technologies in commercial buildings, their performance and affecting factors,” Renewable Sustain. Energy Rev., vol. 33, pp. 268–279, May 2014.

[3] H.H.Kim,K.N.Ha,S.Lee,andK.C.Lee,“Residentlocation-recognitionalgorithm using a Bayesian classifier in the PIR sensor-based indoor location-aware system,” IEEETrans.Syst.,Man,Cybern,CAppl.Rev.,vol.39,no.2,pp.240–245,Mar.2009.

[4] Q.Hao,F.Hu,andY.Xiao,“Multiplehumantrackingandidentificationwithwireless distributed pyroelectric sensor systems,” IEEE Syst. J., vol. 3, no. 4, pp. 428–439, Dec. 2009.

[5] J.-S. Fang, Q. Hao, D. J. Brady, B. D. Guenther, and K. Y. Hsu, “Real-time human identification using a pyroelectric infrared detector array and hidden Markov models,” Opt. Express, vol. 14, no. 15, pp. 6643–6658, 2006.